Reactive convective dissolution with differential diffusivities: Nonlinear simulations of onset times and asymptotic fluxes

M. Jotkar,* L. Rongy,† and A. De Wit‡
Université libre de Bruxelles, Nonlinear Physical Chemistry Unit, Faculté des Sciences, Campus Plaine, C.P. 231, 1050 Brussels, Belgium

(Received 28 May 2020; accepted 28 September 2020; published 19 October 2020)

Convection can develop upon dissolution of a given species A in a host phase when dissolution leads to a buoyantly unstable density stratification. If A reacts with a solute B present in the host solution according to a bimolecular $A + B \rightarrow C$ reaction, convective dissolution can be enhanced or slowed down depending on the relative contribution to density of each chemical species. We study numerically the influence of differential diffusion on such reactive convective dissolution in the nonlinear regime. In particular we compute the temporal evolution of the dissolution flux, its asymptotic value and the onset time of convection as a function of the ratio of the diffusion coefficients. We find that, when B diffuses faster than C, the density profiles can exhibit a local minimum below the reaction front where a double-diffusive instability develops. This has a destabilizing effect and leads to enhanced mixing, earlier onset of convection, and increased asymptotic fluxes. On the other hand, when B diffuses slower than C, the density profiles can contain a local minimum at the reaction front followed by a local maximum below, which gives rise to two convection zones with a diffusive-layer convection instability occurring below the reaction front. The overall dynamics is stabilizing with delayed onset of convection and with smaller asymptotic fluxes. When B and C diffuse at an equal rate but differently from A, differential diffusion can accelerate or slow down convection.

DOI: 10.1103/PhysRevFluids.5.104502

I. INTRODUCTION

Dissolution-driven convection that occurs following the dissolution of a given species into a host phase has been investigated in detail recently due to its relevance in CO_2 geological sequestration. In this technique, CO_2 is captured at production sites, transported through pipelines, and injected into geological storage sites such as saline aquifers [1]. Upon injection, CO_2 rises above the resident fluid up to an impermeable cap rock, such that a two-layer stratification of CO_2 (phase A) overlying brine (host phase) is created. As CO_2 is partially miscible into water, its subsequent dissolution into the brine increases the density of the salt water, which leads to a buoyantly unstable configuration of denser CO_2-rich brine above less dense resident fluid. A buoyancy-driven convective instability sets in, which triggers density fingering that accelerates the transfer of CO_2 towards the trapping host fluid and is thus favorable to the sequestration process [2–9].

Recently, it has been shown that chemistry can have a strong impact on convective dissolution [8,10–28]. More specifically, it has been demonstrated that simple $A + B \rightarrow C$ reactions can modify the characteristics of the fingering instability as they influence the concentration profiles and

*mjotkar@ulb.ac.be
†lrongy@ulb.ac.be
‡adewit@ulb.ac.be

hence the density stratification [28]. When the dissolving species increases the density of the host phase upon dissolution and reacts with B, the $A + B \rightarrow C$ reaction can slow down or accelerate convection depending on the relative Rayleigh number of each species, quantifying its contribution to changes of density in the host solution [12,15,20,26].

Most theoretical studies of this influence of reactions have assumed that all chemical species diffuse equally. However, in practice, the various solutes usually diffuse at different rates and this can have a strong impact, as seen in experiments, on reactive convective dissolution [11,13,17]. It is therefore of interest to quantify how differential diffusivity of the chemical species in the host solution affects the convective dynamics in reactive cases and modifies the amount of CO_2 that can be dissolved in the host phase for a given time.

Differential diffusion can induce additional instabilities [29–32]. In particular, in the case of a less dense solution of a slow diffusing solute above a denser solution of a faster diffusing solute, a double diffusion (DD) instability can destabilize the stratification into fingers extending on average the same distance around the initial position of the contact line [29–31]. In contrast, if the upper less dense solution contains the fastest diffusing solute, a diffusive layer convection (DLC) instability induces separate convective motions both above and below the contact line [31,32]. Hence, as soon as two solutes that diffuse at different rates dissolve in the same host phase, differential diffusion effects can already alter the nonreactive convective dissolution [33]. In reactive convective dissolution, these differential diffusive mechanisms of destabilization can intervene locally in addition to the reaction to modify the convective sinking of denser A from the above interface [24,25,34,35].

The various reaction-diffusion (RD) density profiles that can develop after dissolution of A when the solutes of an $A + B \rightarrow C$ reaction diffuse at different rates have been classified theoretically into various regimes [16,17]. Theoretical studies have shown that differential diffusivity affects the growth rate in the linear regime [25], and accelerates or slows down the onset time for convective instabilities [24,35]. In the case where all species contribute equally to density, differential diffusivities can moreover give rise to new dynamics, including the presence of two different convection zones when a nonmonotonic density profile with both a minimum and a maximum develops [24,35]. Double diffusion can also induce the onset of an instability in regions where locally a less dense solution lies above a denser one [24,34,35]. However, in most of those works, the density contribution of either the reactant A or B and product C were maintained equal to focus on the differential diffusivity effects. Moreover, nonlinear dynamics have been studied but the impact of differential diffusion on asymptotic fluxes is poorly understood.

In this regard, several open questions remain, as an extensive part of the parameter space is still unexplored. For example, what is the effect of varying diffusivities on the nonlinear dynamics when the density contribution of all species is different? Second, the cases where B and C diffuse equally but differently from A have not been investigated. In addition, the impacts of differential diffusivity on the temporal evolution of the dissolution flux, on its asymptotic value, and on the onset time of convection are not known in detail. We address all these questions here.

To do so, we numerically study dissolution-driven convection in two partially miscible phases when the dissolving phase A introduced from above increases the density of the host phase upon dissolution. A then reacts with B to produce C due to an $A + B \rightarrow C$ type of a reaction. All three species contribute to the density of the host solution and diffuse at different rates. While the equivalent equal diffusion scenario has been investigated in detail in Ref. [26], we consider here two particular representative cases when C is either denser or less dense than B with characteristically distinct dynamics and vary the diffusivities of the species. We focus here on analyzing the effect of differential diffusivity on the morphology of the fingering instability, on its onset time and on the dissolution flux of A. Our objective is to highlight for two representative scenarios the specific nonlinear dynamics developing when either DD or DLC convection develops below the reaction front while the Rayleigh-Taylor instability is present above the front.

The article is organized as follows. In Sec. II we explain the numerical model used. In Sec. III we classify the reaction-diffusion density profiles into the various regimes. In Sec. IV we analyze

the nonlinear convective dynamics and in Sec. V we present quantitative results for the dissolution fluxes, their asymptotic value, and the onset time for convection. Finally, we highlight our main findings in Sec. VI.

II. PROBLEM FORMULATION

We consider a homogeneous, isotropic, isothermal porous medium in which two partially miscible phases are initially separated by a horizontal interface [16,24]. The gravitational field $\bar{\mathbf{g}}$ points downwards along the vertical z' axis and is perpendicular to the horizontal x' axis. The phase A dissolves from above into the host phase containing a reactant B with an initial concentration B_0 to generate a product C via a second-order $\mathrm{A}+\mathrm{B}\rightarrow\mathrm{C}$ reaction. For example, in some experiments [12,17,23], $\mathrm{A}=\mathrm{CO_2}$, water is the solvent of the host phase, B = alkaline hydroxides (like LiOH, NaOH for instance), and the products C formed are carbonate salts (like $\mathrm{Li_2CO_3}$ or $\mathrm{Na_2CO_3}$ for example). In other experiments [11,23], the reactant A is an ester which, upon dissolution in water, reacts with B = alkaline hydroxide to yield products C such as a salt and an alcohol. Independently of the details of the reaction, what matters is that all species contribute to the solution density. We assume a local chemical equilibrium such that the concentration of A at the interface ($z'=0$) remains constant in time and is equal to its finite solubility A_0 in the host phase. The concentrations of B and C are assumed to be small enough not to affect this solubility. The host phase extends from $x'=0$ to $x'=L'$ in the horizontal direction and from $z'=0$ to $z'=H'$ in the vertical direction. We focus here on the effect of differential diffusivities of the three species on the density stratification that is already unstable in the absence of reactions, i.e., when the dissolving phase A increases the density of the host phase upon dissolution from above.

The solute concentrations, time, spatial coordinates, and velocity are nondimensionalized as [20,26]

$$A=A'/A_0,\quad B=B'/A_0,\quad C=C'/A_0, \tag{1a}$$

$$t=t'/t_c,\quad z=z'/l_c,\quad \mathbf{u}=\mathbf{u}'/u_c, \tag{1b}$$

where the primes denote dimensional quantities and $\mathbf{u}=(u,v)$ is the two-dimensional velocity field. The chemical timescale $t_c=1/(qA_0)$ with q the kinetic constant of the reaction, the reaction-diffusion (RD) length scale $l_c=\sqrt{D_A t_c}=\sqrt{D_A/(qA_0)}$ with D_A the diffusion coefficient of A, and the velocity scale $u_c=\phi l_c/t_c=\phi\sqrt{D_A q A_0}$ with ϕ the porosity of the medium.

The dimensionless reaction-diffusion-convection (RDC) equations governing the temporal evolution of the solute concentrations read as

$$\frac{\partial A}{\partial t}+(\mathbf{u}\cdot\boldsymbol{\nabla})A=\nabla^2 A-AB, \tag{2a}$$

$$\frac{\partial B}{\partial t}+(\mathbf{u}\cdot\boldsymbol{\nabla})B=\delta_B\nabla^2 B-AB, \tag{2b}$$

$$\frac{\partial C}{\partial t}+(\mathbf{u}\cdot\boldsymbol{\nabla})C=\delta_C\nabla^2 C+AB, \tag{2c}$$

where $\delta_B=D_B/D_A$ and $\delta_C=D_C/D_A$, with D_B and D_C the diffusion coefficients of species B and C, respectively.

The RDC equations (2) are complemented by Darcy's law for the velocity $\mathbf{u}=(u,v)$ of an incompressible flow in a porous medium, given as

$$\boldsymbol{\nabla}p=-\mathbf{u}+\rho\mathbf{e}_z, \tag{3}$$

with p the dimensionless pressure and $\mathbf{e}_z$ the unit vector along the gravity field.

A linear equation of state expresses the dependence of the dimensionless density ρ of the host solution on concentrations:

$$\rho = R_A A + R_B B + R_C C, \tag{4}$$

where the Rayleigh numbers R_i $(i = A, B, C)$ quantify the contribution to density of the species i as

$$R_i = \frac{\alpha_i A_0 g \kappa}{\phi \nu \sqrt{D_A q A_0}}, \tag{5}$$

where $\alpha_i = \frac{1}{\rho_0}\frac{\partial \rho'}{\partial c_i'}$ is the solutal expansion coefficient of species i, ρ_0 is the dimensional density of the solvent, κ is the permeability, and ν is the kinematic viscosity of the solvent.

Periodic boundary conditions are imposed at $x = 0$ and $x = L$; no vertical flow and no flux conditions are used for A, B, and C at $z = H$ (bottom boundary) while at $z = 0$ (interface) we use no vertical flow and no flux conditions for B and C along with $A = 1$. We solve Eqs. (2) and (3) using the following initial conditions:

$$A(x, z = 0, t = 0) = 1 + \epsilon \cdot \text{rand}(x), \quad A(x, z > 0, t = 0) = 0, \tag{6a}$$

$$B(x, z, t = 0) = \beta, \tag{6b}$$

$$C(x, z, t = 0) = 0. \tag{6c}$$

where $\beta = B_0/A_0$ is the ratio of the initial concentration of B and the solubility of A. Perturbations are introduced in the initial concentration of A at the interface [Eq. (6a)] in order to trigger the instability [36,37]. The amplitude of the perturbations is $\epsilon \sim 10^{-3}$ and rand(x) is their modulation along x, varying randomly between -1 and 1 ("white noise").

If all diffusion coefficients are different, the problem is controlled by six parameters: δ_B, δ_C, R_A, R_B, R_C, and β. If all species diffuse at equal rates ($\delta_B = \delta_C = 1$), a conservation relation can be used to reduce the number of parameters to three: R_A, $\Delta R_{CB} = R_C - R_B$, and β [12,20]. The nonlinear dynamics for such equal diffusion scenarios have been investigated in detail for initially unstable density stratifications with $R_A = 1$ in Refs. [20,26] and for initially stable density stratifications with $R_A = -1$ in Refs. [20,38] for a range of ΔR_{CB} and β. We study here the effect of differential diffusivities on the convective dynamics in a density stratification that is unstable in the absence of reactions ($R_A > 0$). More specifically, we focus here on two representative cases from [20] with characteristically distinct dynamics when C is either denser ($R_C > R_B$) or less dense than B ($R_C < R_B$) and vary the relative diffusivities of the species. To do so, we fix $R_A = 1$ and $\beta = 1.5$ throughout this article and vary δ_B, δ_C, R_B, and R_C.

We solve the RDC equations (2) numerically along with Eqs. (3) and (4) using relevant boundary conditions and YALES2 [39] software with the DARCY_SOLVER module. Computational domain width $L = 3072$ and height $H = 2048$ are used for $R_B/R_C = 2$ while for $R_B/R_C = 0.5$ a larger domain height $H = 4096$ is used to ensure that the results are independent of the domain size. The reader may refer to Refs. [19,20,24] for further details on the numerics.

III. CLASSIFICATION OF THE DENSITY PROFILES

Figure 1 shows typical RD concentration profiles in a host phase when A dissolves from above and reacts according to an A + B → C scheme with a solute B to produce C at the reaction front. The region between the interface and the reaction front mainly consists of A and C. At the front, A and B are consumed to generate C, while the bulk is essentially a solution of B. We show here that, when all the species diffuse differently, it gives rise to distinct dynamics above and below the reaction front. The region above the reaction front is dominated by the classical Rayleigh-Taylor (RT) instability occurring due to a denser A-rich layer lying on top of a less dense one. Below the reaction front, either a DD or a DLC instability can occur between the upper C-rich zone and the lower B-rich bulk due to differential diffusion.

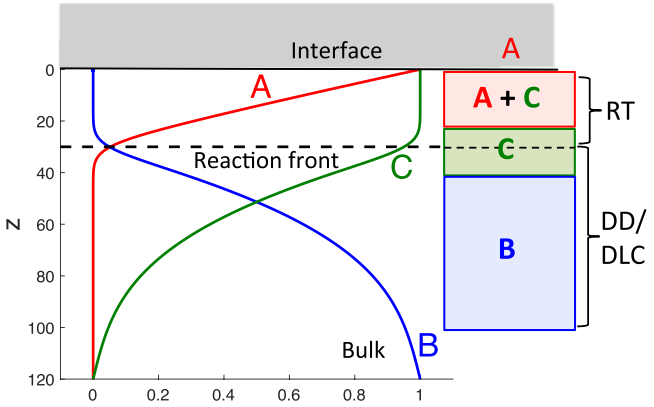

FIG. 1. Reaction-diffusion (RD) concentration profiles for species A, B, and C developing upon dissolution of A from above in a host phase containing B, followed by an A + B → C reaction. The dashed line represents the location of the reaction front where C is produced by the reaction. The zone between the interface and the reaction front contains mainly A and C while only B is present far away in the bulk. Here $\beta = 1$. The right part of the figure depicts schematically the different zones of composition below the interface with the possible instabilities.

To understand the differential diffusivity effects on the convective dynamics, we first recall that the different types of density profiles and the related qualitative behavior of the fingering dynamics depend only on the relative values of the Rayleigh numbers and diffusion coefficients. Hence, they can be classified in the $(R_B/R_C,\ \delta_B/\delta_C)$ parameter space as shown in Fig. 2 [16,24]. For equal diffusion coefficients and C denser than B ($R_B/R_C \leqslant 1$, pink line), the density profiles

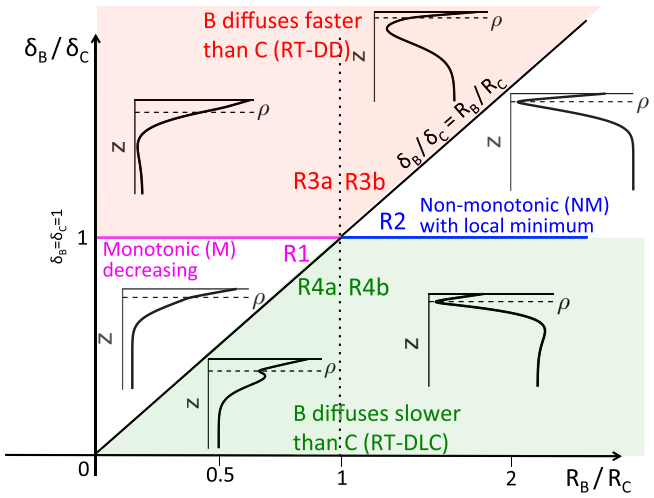

FIG. 2. Classification of the RD density profiles $\rho(z)$ in the $(R_B/R_C,\ \delta_B/\delta_C)$ space for $R_A, R_C > 0$. The dashed black lines on the density sketches represent the location of the reaction front. Regimes are R1 (monotonic decreasing), R2 (minimum at the reaction front), R3a, R3b (minimum below the reaction front), R4a, R4b (minimum at the reaction front followed by a maximum below). The equal diffusivity cases from Ref. [26] are indicated by the horizontal line with $\delta_B = \delta_C = 1$; those when C is denser or less dense than B, with density profiles similar to regimes R1 and R2, are indicated by the pink and blue lines, respectively. Adapted from Refs. [16,24].

are monotonically (M) decreasing, giving rise to strong convection [26]. Conversely, when C is less dense than B ($R_B/R_C > 1$, blue line), the density profiles are nonmonotonic (NM) with a local minimum, which creates a barrier for the fingers and prohibits their progression. As a consequence, the fingers remain stuck close to the interface up to very large times [26]. If the chemical species diffuse at different rates, regimes R1 ($R_B/R_C < \delta_B/\delta_C < 1$) with monotonically decreasing profiles and R2 ($1 < \delta_B/\delta_C < R_B/R_C$) with nonmonotonic profiles containing a local minimum at the reaction front give rise to dynamics qualitatively similar to the equal diffusivity cases [24,26].

We identify four other regimes where the density profiles are different from those of the equal diffusivity case. For C denser than B ($R_B/R_C \leqslant 1$), either B diffuses faster than C and we are in regime R3a ($\delta_B/\delta_C > 1$) with a local minimum below the reaction front, or C is the fast diffusing species and we are in regime R4a ($\delta_B/\delta_C < R_B/R_C < 1$) with a local minimum at the reaction front followed by a local maximum below it and the interface value of ρ is larger than its value in the bulk.

For C less dense than B ($R_B/R_C > 1$), regime R3b ($\delta_B/\delta_C > R_B/R_C > 1$) has density profiles with a local minimum of large intensity below the reaction front, while regime R4b ($\delta_B/\delta_C < 1$) features a local minimum at the reaction front followed by a local maximum below it and the interface value of density is smaller than the bulk density.

In regime R3 ($\delta_B/\delta_C > \max[1, R_B/R_C]$), the density profiles exhibit a local minimum similar to regime R2 but this minimum is located below the reaction front rather than at the reaction front. Compared to the equal diffusion case, the slowest diffusing product C is present more abundantly at the reaction front where it is produced and less in the bulk since it diffuses slowly. If C is sufficiently dense, i.e., $R_C > R_B\delta_C/\delta_B$, it creates a local depletion below the front since B is consumed by the reaction and this leads to a RT instability above the reaction front and a DD instability below it. The dynamics is governed by a coupled RT-DD mechanism in the red region in Fig. 2 as B diffuses sufficiently faster than C.

On the other hand, in regime R4 ($\delta_B/\delta_C < \min[1, R_B/R_C]$), the density profiles have a minimum at the reaction front followed by a local maximum below it. This local maximum is caused by the local accumulation of B below the reaction front if B diffuses slower and contributes to the density sufficiently. A RT instability then develops above the reaction front and a DLC instability below it. The convective pattern is thus dominated by coupled RT-DLC mechanisms in the green region in Fig. 2.

We have classified the RD density profiles into different regimes. In the next section, we study the nonlinear convective dynamics for specific cases in regimes R3 and R4.

IV. NONLINEAR CONVECTIVE DYNAMICS

We now analyze differential diffusivity effects on the nonlinear convective dynamics successively for representative cases when C is denser and less dense than B.

A. C denser than B ($R_B/R_C \leqslant 1$)

We first consider the case where C is denser than B, for example $R_B/R_C = 0.5$ ($R_B = 1, R_C = 2$). We recall that this case corresponds to monotonically decreasing density profiles when all species diffuse equally. Figure 3 compares the density fields at different times. In the top line, B and C diffuse at equal rate. The spatiotemporal development of the fingering instability is qualitatively similar to the nonreactive [5] and reactive [20,26] cases. Initially, the dynamics is dominated by diffusion. At a time close to 700 (not shown here), fingers appear with a given wavelength (linear growth regime). Afterwards, the fingers merge increasing the wavelength and new protoplumes are generated regularly at the boundary layer in the reinitiation regime before merging with the existing older fingers.

A case where B diffuses faster than C (regime R3a) is shown in the middle row of Fig. 3. The density profiles contain in that case a local minimum below the reaction front. The fingering

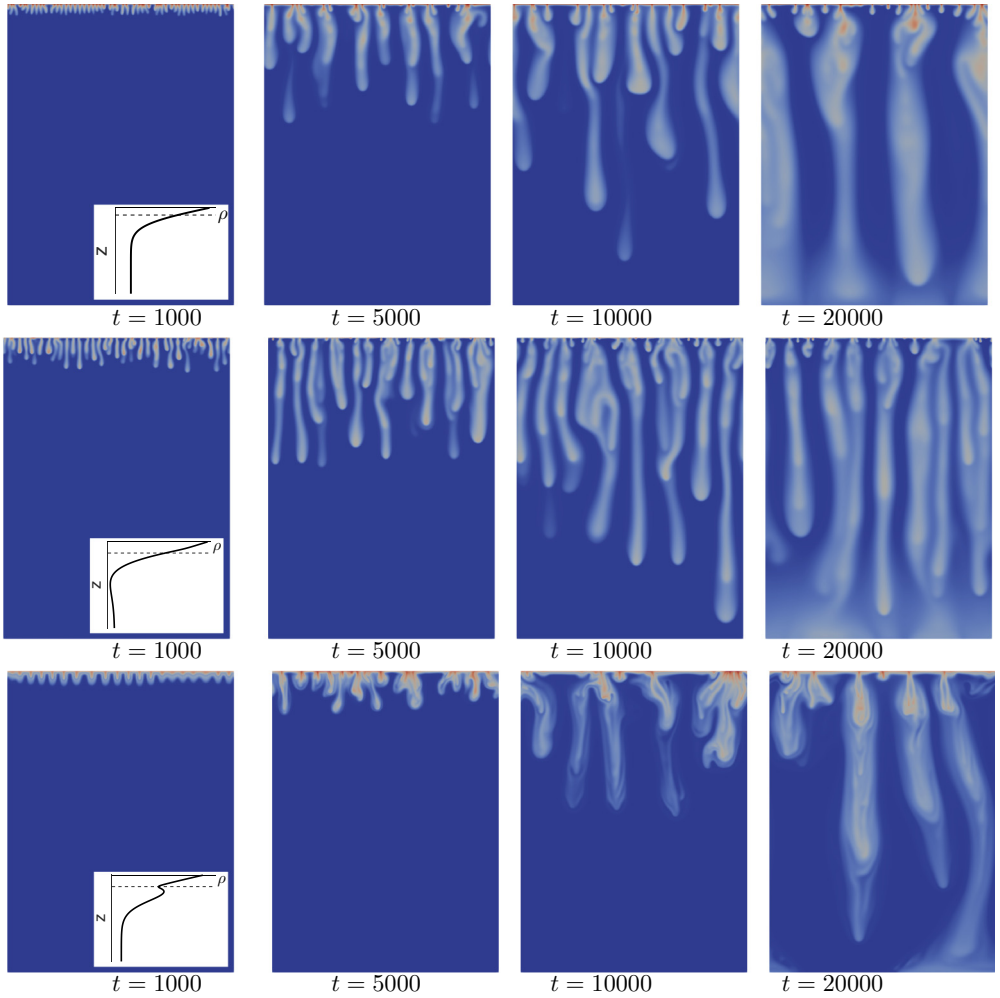

FIG. 3. Density ρ field at different times t for $R_B = 1$, $R_C = 2$, $\delta_C = 1$ with (top) $\delta_B = 1$: in regime R1; (middle) $\delta_B = 3$: RT-DD case in regime R3a; (bottom) $\delta_B = 0.33$: RT-DLC case in regime R4a. Typical RD density profiles are shown in the left panels. Density scales between its minimum (blue) and maximum (red) values in each line. Note that the effect of differential diffusivities is stronger for $\beta = 1$ [24].

instability occurs sooner but merging and reinitiation are also observed. Typically, in this regime the stabilizing barrier created by the less dense fluid lying locally on top of the denser one prohibits the downward movement of the fingers, resulting in fingers that are thicker above the local minimum and narrower below it [24]. This effect increases with R_B/R_C. However, for the particular $R_B/R_C = 0.5$ and $\beta = 1.5$ chosen here, the barrier is weak and causes the fingers to be only slightly narrower below the reaction front. Although there exists a weak DD instability below the reaction front due to B diffusing faster than C, the overall dynamics is dominated by RT instability while the effect of differential diffusion is stronger for $\beta = 1$.

Conversely, when B diffuses slower than C (regime R4a shown in the lower line of Fig. 3), the density profiles contain a local minimum at the reaction front followed by a local maximum below it. The density at the interface is larger than in the bulk and the overall dynamics is dominated by the RT instability. However, below the reaction front, there exists a region with, locally, a less dense solution of the fast-diffusing C above the denser solution of the slow-diffusing B. This is prone to

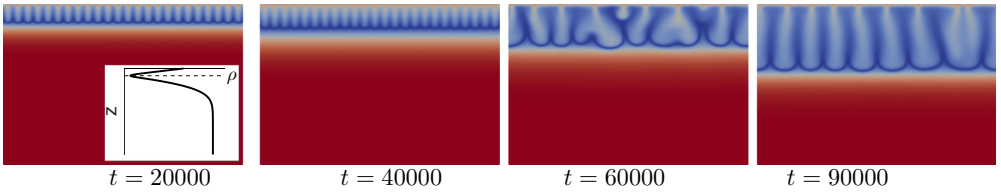

FIG. 4. Density ρ field at different times t for $R_B = 2$, $R_C = 1$, $\delta_C = \delta_B = 1$. A typical RD density profile is shown in the left panel. Density scales between -1.5 (blue) and 0 (red).

weak DLC inducing a secondary convective zone with antenna-like structure at the tips of the RT fingers [32].

B. C less dense than B ($R_B/R_C > 1$)

Let us now consider the case where C is less dense than B, for example $R_B/R_C = 2$ ($R_B = 2, R_C = 1$). When all species diffuse at the same rate, the density profiles are nonmonotonic with a local minimum (Fig. 4). The density at the interface is smaller than the bulk value. The minimum in density creates a barrier and the fingers remain stuck close to the interface up to very large times. At a time close to 60 000, the fingers merge such that a pattern with few regular fingers is obtained.

When B diffuses faster than C in regime R3b, the density fields contain a local minimum below the reaction front and the density at the interface is larger than far away in the bulk (Fig. 5 top). The stratification of the denser fluid layer rich in A above the less dense reaction front containing A and C develops primary fingers due to the RT instability. Below the reaction front, the less dense solution of the slow-diffusing C overlies the denser solution of the fast-diffusing B, which leads to

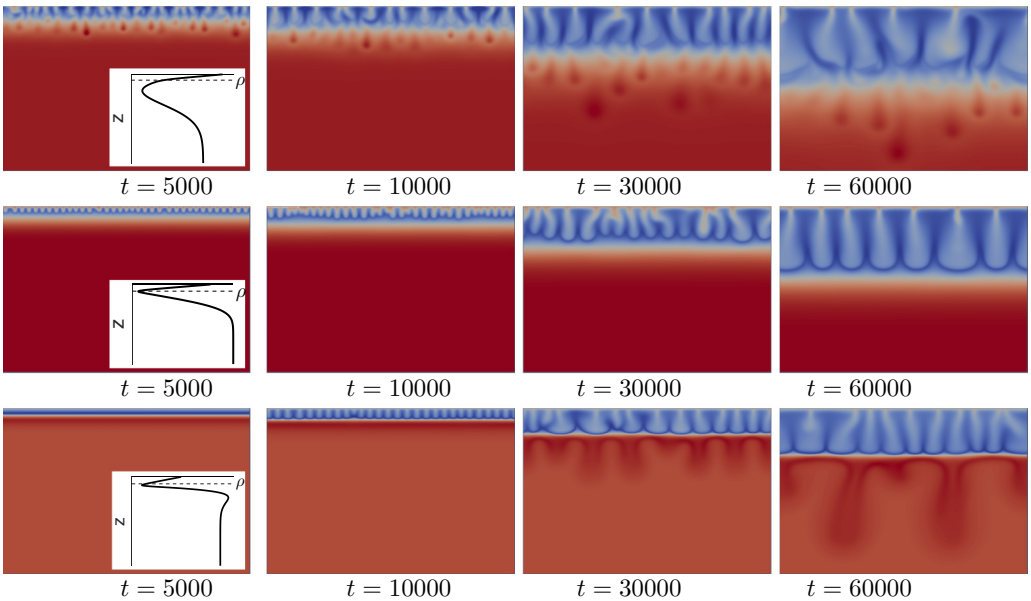

FIG. 5. Density ρ field at different times t for $R_B = 2$, $R_C = 1$, $\delta_C = 1$ with (top) $\delta_B = 3$: RT-DD case in regime R3b; (middle) $\delta_B = 3/2$: in regime R2; (bottom) $\delta_B = 1/3$: RT-DLC case in regime R4b. Typical RD density profiles are shown in the left panels. Density scales between its minimum (blue) and maximum (red) values in each line.

a DD instability with secondary fingers sinking below the tips of the primary ones. The convective instability sets in sooner, and both the primary and secondary fingers merge in time and sink rapidly towards the bottom. In regime R2 (Fig. 5 middle), although the dynamics are qualitatively similar to the equal diffusion scenario, a weak DD instability influences the asymptotic regime as the fingers merge to a larger wavelength sooner.

If B diffuses slower than C in regime R4b (Fig. 5 bottom), the density profiles contain a local minimum at the reaction front followed by a local maximum below it and the density at the interface is smaller than its bulk value. After the initial diffusive transient, the convective instability occurs later in time followed by the merging of the fingers. We observe two zones of convection, respectively above and below the reaction front separated by a light blue boundary corresponding to the location of the local minimum in density. Above the reaction front the primary fingering is due to a RT instability, while below the reaction front a secondary convective pattern marked by DLC-driven antennalike structures arises where the less dense solution of the fast-diffusing C overlies the denser solution of the slow-diffusing B.

In summary, when B diffuses faster than C, the dynamics are governed by coupled RT and DD modes while, in the reverse case where B diffuses slower than C, RT and DLC mechanisms govern the nonlinear convection, for both C denser and less dense than B. In the following section, we quantify the impact of these mechanisms on the dissolution flux of the dissolving species A.

V. DISSOLUTION FLUX WITH DIFFERENTIAL DIFFUSIVITIES

Let us here examine the impact of differential diffusivities on the temporal evolution of the dissolution flux, on its asymptotic value and on the onset time for convection for various values of the control parameters.

The storage capacity of the dissolving species A in the host solution can be quantified on the basis of the dissolution flux J, defined as

$$J = -\frac{1}{L}\int_0^L \left.\frac{\partial A}{\partial z}\right|_{z=0} dx. \tag{7}$$

The temporal evolution of the dissolution flux J is shown in Fig. 6 when C is denser than B and in Fig. 7 when C is less dense than B for various couples of differential diffusivities (δ_B, δ_C). Solid black curves in both figures correspond to the equal diffusivity case. One curve represents the average over 15 simulations with different realizations of the initial noise of the same amplitude shown in Eq. (6a). The 95% confidence interval shown as lighter areas around the curves represents the variability due to the random noise on the initial condition. Initially, the flux J follows the decreasing diffusive trend until it increases again due to the onset of convection. Eventually, it fluctuates around an asymptotic value J^*. This is qualitatively similar to nonreactive [5] and reactive scenarios when all species diffuse equally [20,26].

When C is denser than B, the dissolution flux peaks at two values because of merging of fingers before reaching an asymptotic constant value J^* for equal diffusivities (Fig. 6). For B diffusing faster than C in regime R3a (Fig. 6 top), the dynamics is governed by the RT instability above and the DD instability below the reaction front. Initially, at the reaction front, the fast-diffusing B is easily available for consumption by the reaction. This accelerates convection because it produces a denser species C. Hence, the flux J departs sooner from the diffusive trend. However, due to the barrier created by the local minimum in the density profiles below the reaction front, the asymptotic fluxes are lower than that of the equal diffusivity case. Note that, while the ratio $\delta_B/\delta_C > 1$ fixes the qualitative type of RT-DD dynamics, the quantitative values of the flux and in particular its asymptotic value vary with the absolute values of δ_B and δ_C for a given ratio δ_B/δ_C (see Fig. 6).

On the other hand, for B diffusing slower than C in regime R4a (Fig. 6 bottom), the DLC instability occurring below the reaction front influences the RT instability. Since B is slow diffusing, it is less easily available for consumption by reaction at the reaction front, and the onset of

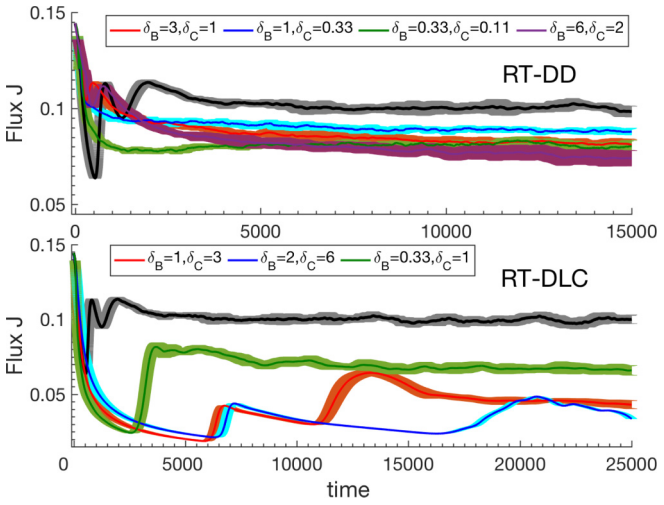

FIG. 6. Temporal evolution of the dissolution flux J for C denser than B ($R_B/R_C = 0.5$) and different diffusivities (δ_B, δ_C) indicated in the inset: (top) $\delta_B/\delta_C = 3$: RT-DD case in regime R3a; and (bottom) $\delta_B/\delta_C = 1/3$: RT-DLC case in regime R4a. Solid black curves correspond to the equal diffusivity case with $\delta_B = \delta_C = 1$ [26].

convection is delayed. Moreover, the asymptotic fluxes are lower. For a fixed ratio of $\delta_B/\delta_C = 1/3$, we see that, again, the intensity of the flux varies with the absolute values of δ_B and δ_C and that the largest asymptotic flux is obtained for the lowest absolute values of δ_B and δ_C. This relates to the fact that the slower the product C diffuses, the denser is the upper solution and thus the more efficient is the RT instability.

When C is less dense than B (Fig. 7) but diffuses at the same rate, the flux J peaks close to the onset of instability, followed by an intermediate diffusivelike scaling with time up to $t \sim 50\,000$,

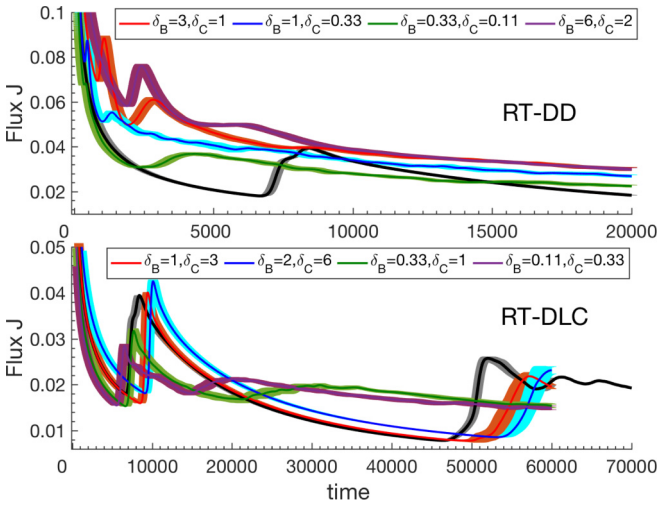

FIG. 7. Temporal evolution of the dissolution flux J for C less dense than B ($R_B/R_C = 2$) and different diffusivities (δ_B, δ_C) indicated in the inset: (top) $\delta_B/\delta_C = 3$: RT-DD case in regime R3b; and (bottom) $\delta_B/\delta_C = 1/3$: RT-DLC case in regime R4b. Solid black curves correspond to the equal diffusivity case with $\delta_B = \delta_C = 1$ [26].

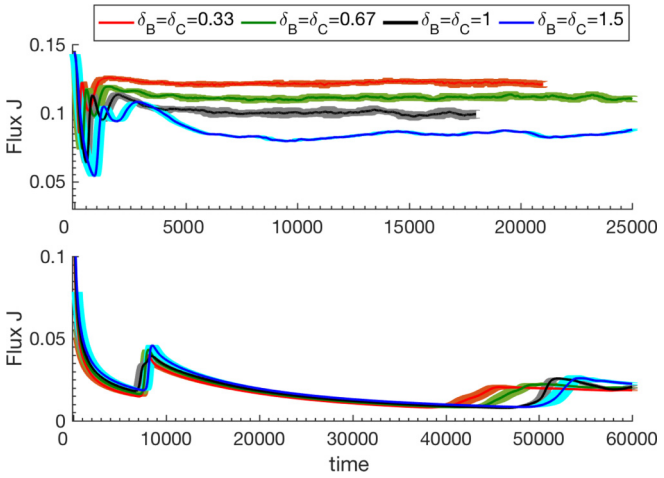

FIG. 8. Temporal evolution of flux J for different values of $\delta_B = \delta_C$ indicated in the inset for (top) C denser than B with $R_B/R_C = 0.5$ and (bottom) C less dense than B with $R_B/R_C = 2$.

after which the fingers merge, inducing the flux to reach an asymptotic limit J^*. The temporal evolution of fluxes for B diffusing faster than C in regime R3b is shown in Fig. 7 top. The convective dynamics dictated by the RT-DD interplay and the fact that the fast-diffusing B is easily consumed by the reaction accelerate the onset of convection. The asymptotic fluxes are also larger than the equal diffusion one. In contrast, when B diffuses slower than C in regime R4b (Fig. 7 bottom), the dynamics are slowed down slightly due to the RT-DLC interplay. However, the impact of differential diffusivities for this specific set of parameters is relatively weak. Here again, the J^* values vary with the absolute values of δ_B and δ_C for a fixed ratio of δ_B/δ_C.

Eventually, let us consider the case where B and C diffuse at the same rate but differently from A. Figure 8 top corresponds to C denser than B with monotonically decreasing density profiles. When B and C diffuse slower than A, i.e., $\delta_B = \delta_C < 1$, more C remains present in the upper layer. This increases the intensity of the unstable density stratification and leads to an earlier onset of convection and higher asymptotic fluxes as seen here. Conversely, when B and C both diffuse faster than A, i.e., $\delta_B = \delta_C > 1$, C diffuses rapidly downwards, which has a stabilizing effect on the flux with a delayed onset of convection and a lower asymptotic flux.

Similarly, Fig. 8 bottom corresponds to C less dense than B with nonmonotonic density profiles. The local minimum in the density creates a barrier prohibiting the progression of the fingers. When B and C diffuse at the same rate but slower than A, i.e., $\delta_B = \delta_C < 1$, C acts more in the upper layer. This has a mild destabilizing effect, which promotes the merging of fingers sooner, as seen in the earlier occurrence of the second peak in the values of J. Conversely, when B and C diffuse at the same rate but faster than A, i.e., $\delta_B = \delta_C > 1$, this causes a slight delay in the merging of the fingers. However, the asymptotic flux values are the same for all $\delta_B = \delta_C$.

We now analyze the onset time for convection t_0, defined based on the magnitude of the velocity field computed as $U^2(t) = \int_0^H \int_0^L [u^2(x,z,t) + v^2(x,z,t)]dx\,dz$. Typically, U^2 decreases in the diffusive limit until a given onset time t_0. It reaches the minimum before U^2 begins to grow due to the onset of convection [5,20]. The onset time t_0 is given in Fig. 9 for all the diffusivities studied here with C both denser and less dense than B. We observe that t_0 can be reduced up to an order of magnitude when B diffuses faster than C (regime R3) when RT and DD instabilities work cooperatively. This has an overall destabilizing effect on the dynamics. Conversely, when B diffuses slower than C (regime R4), the coupled RT and DLC dynamics have a stabilizing effect amounting to a general trend of increasing t_0. We note, however, that for both C denser and less dense than B the absolute values of diffusivities (δ_B, δ_C) have a strong impact on t_0 in addition to

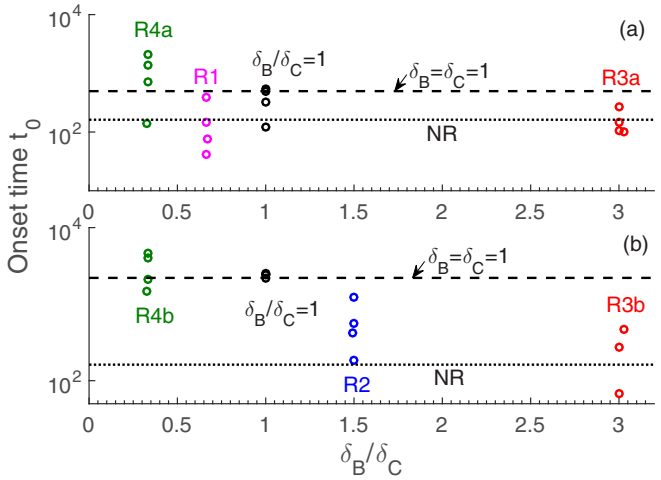

FIG. 9. Onset time t_0 for different diffusivity ratios δ_B/δ_C when (a) C is denser than B ($R_B/R_C = 0.5$) and (b) C is less dense than B ($R_B/R_C = 2$). Dashed lines represent the equal diffusion cases while the dotted lines correspond to the nonreactive (NR) case. For a given ratio of δ_B/δ_C, various combination of absolute values of diffusivities (δ_B, δ_C) are used.

the ratio δ_B/δ_C relative to R_B/R_C. This effect is also observed on the flux (Figs. 6 and 7) whose values depend on the diffusivities and not only on the ratio δ_B/δ_C.

Next, we quantify the long-term fate of species A in a given host phase by inspecting the asymptotic values of J^* as a function of δ_B/δ_C in Fig. 10. Once again, in regimes R3 with RT-DD interplay, the asymptotic fluxes J^* can be increased relative to the equal diffusivity ones for C less dense than B. However, J^* is lower than the equal diffusion one for C denser than B. The reason for this may be attributed to the barrier created in the local minimum below the reaction that slows down the dynamics relative to the equal diffusion one. Conversely, in regimes R4, where RT-DLC

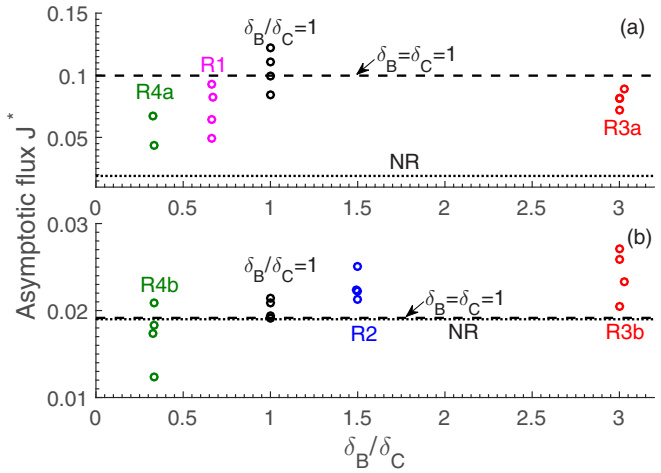

FIG. 10. Asymptotic flux J^* for different diffusivity ratios δ_B/δ_C when (a) C is denser than B ($R_B/R_C = 0.5$) and (b) C is less dense than B ($R_B/R_C = 2$). Dashed lines represent the equal diffusion cases and dotted lines represent the nonreactive (NR) case. For a given ratio of δ_B/δ_C, various combination of absolute values of diffusivities (δ_B, δ_C) are used.

mechanisms dominate the dynamics, the J^* values are mainly lower than the equal diffusion ones due to the slow-diffusing B in the bulk.

We have thus shown that regime R3 has a destabilizing effect on the convective dynamics due to the RT-DD mechanism whereas regime R4 has a stabilizing effect due to the RT-DLC mechanism. Differential diffusivities have thus a significant impact on the storage rates and it is therefore possible to accelerate the onset of convection when B diffuses faster than C.

VI. CONCLUSIONS

We have numerically studied the effect of differential diffusion on nonlinear convective dissolution when the dissolving species A increases the density of the host phase upon dissolution and reacts with B to produce C via an $A + B \rightarrow C$ reaction. All species diffuse at different rates and contribute to the density of the host solution. We have focused our study on two representative cases: when C is either denser or less dense than B with $R_A = 1$ and $\beta = 1.5$. We have classified the dynamics into different regimes based on the morphology of the fingering pattern and the density profiles. We have quantified the dissolution fluxes, onset times for convection, and asymptotic fluxes to show that differential diffusivities can impact storage rates significantly and, therefore, need to be taken into account for accurately predicting the efficiency of the sequestration technique.

When B diffuses faster than C, the density profiles contain a local minimum below the reaction front. This leads to dynamics governed by a Rayleigh-Taylor instability above and a double-diffusive instability below the reaction front (RT-DD). The latter is due to the presence of a less dense layer of slow-diffusing C on top of a denser layer containing the fast-diffusing B. This has an overall destabilizing effect relative to the equal diffusion scenarios. For the specific initial concentration of B chosen here, $\beta = 1.5$, we show that when C is denser than B, the DD instability is weak, and the dynamics is dominated by the RT instability. In contrast, when C is less dense than B, the slow dynamics occurring with equal diffusivity can be accelerated with the help of the RT-DD interplay.

Conversely, when B diffuses slower than C, the density profiles contain a local minimum at the reaction front followed by a local maximum below it. Below the reaction front, there exists a less dense layer of fast-diffusing C lying on top of a denser layer containing the slow-diffusing B. This gives rise to two distinct convection zones with a Rayleigh-Taylor instability above and a diffusive-layer convection mode below the reaction front (RT-DLC) that have a stabilizing effect on the convective dynamics. For the specific parameters chosen here, the DLC mode is weak when C is denser than B, but when C is less dense than B the antenna-shaped structures formed below the reaction front slow down the dynamics compared to the equal diffusion case.

Next, we have quantified the dissolution fluxes to demonstrate the destabilizing effect of B diffusing faster than C (RT-DD) and the stabilizing effect of B diffusing slower than C (RT-DLC). We have also studied the effect of B and C diffusing at a same rate different from that of A. We see then that the dissolution fluxes are larger when B and C both diffuse slower than A. We have shown that the onset time t_0 can be reduced up to an order of magnitude when B diffuses faster than C. Similarly, we have measured the asymptotic fluxes J^* determining the long-term fate of the dissolving species A. Although we do not observe a significant increase in J^* for B diffusing faster than C when C is denser than B, we show that J^* can be increased significantly when C is less dense than B. Lastly, we have shown that varying the absolute values of diffusivities (δ_B, δ_C) also impacts the dynamics and dissolution fluxes, in addition to the relative ratios of Rayleigh numbers R_B/R_C and diffusivities δ_B/δ_C.

To summarize, we have shown that differential diffusivities impact the convective dynamics substantially giving rise to additional convective effects below the reaction front. In particular, we have demonstrated that reactant B diffusing faster than product C has a destabilizing effect and, conversely, B diffusing slower than C is stabilizing. Our results are crucial in the context of CO_2 sequestration for accurately modeling convective dissolution and realistically predicting its efficiency as it is most likely that the solutes in the host phases diffuse at different rates.

ACKNOWLEDGMENTS

We would like to thank B. Knaepen and V. Loodts for their help and support concerning the YALES2 code. We gratefully acknowledge the financial support from the Fondation ULB and from the FRS-FNRS PDR CONTROL project.

[1] *Intergovernmental Panel on Climate Change (IPCC) special report on Carbon Dioxide Capture and Storage* (Cambridge University Press, New York, 2005).

[2] G. S. Pau, J. B. Bell, K. Pruess, A. S. Almgren, M. J. Lijewski, and K. Zhang, High-resolution simulation and characterization of density-driven flow in CO_2 storage in saline aquifers, Adv. Water Resour. **33**, 443 (2010).

[3] M. T. Elenius and K. Johannsen, On the time scales of nonlinear instability in miscible displacement porous media flow, Comput. Geosci. **16**, 901 (2012).

[4] A. C. Slim, M. M. Bandi, J. C. Miller, and L. Mahadevan, Dissolution-driven convection in a Hele-Shaw cell, Phys. Fluids **25**, 024101 (2013).

[5] A. C. Slim, Solutal-convection regimes in a two-dimensional porous medium, J. Fluid Mech. **741**, 461 (2014).

[6] H. E. Huppert and J. A. Neufeld, The fluid mechanics of carbon dioxide sequestration, Annu. Rev. Fluid Mech. **46**, 255 (2014).

[7] H. Emami-Meybodi, H. Hassanzadeh, C. P. Green, and J. Ennis-King, Convective dissolution of CO_2 in saline aquifers: Progress in modeling and experiments, Int. J. Greenhouse Gas Control **40**, 238 (2015).

[8] A. De Wit, Chemo-hydrodynamic patterns in porous media, Phil. Trans. R. Soc. A **374**, 20150419 (2016).

[9] C. Thomas, S. Dehaeck, and A. De Wit, Convective dissolution of CO_2 in water and salt solutions, Int. J. Greenhouse Gas Control **72**, 105 (2018).

[10] J. Ennis-King and L. Paterson, Coupling of geochemical reactions and convective mixing in the long-term geological storage of carbon dioxide, Int. J. Greenhouse Gas Control **1**, 86 (2007).

[11] M. A. Budroni, L. A. Riolfo, L. Lemaigre, F. Rossi, M. Rustici, and A. De Wit, Chemical control of hydrodynamic instabilities in partially miscible two-layer systems, J. Phys. Chem. Lett. **5**, 875 (2014).

[12] V. Loodts, C. Thomas, L. Rongy, and A. De Wit, Control of Convective Dissolution by Chemical Reactions: General Classification and Application to CO_2 Dissolution in Reactive Aqueous Solutions, Phys. Rev. Lett. **113**, 114501 (2014).

[13] C. Wylock, A. Rednikov, B. Haut, and P. Colinet, Nonmonotonic Raleigh-Taylor instabilities driven by gas-liquid CO_2 chemisorption, J. Phys. Chem. B **118**, 11323 (2014).

[14] S. S. S. Cardoso and J. T. H. Andres, Geochemistry of silicate-rich rocks can curtail spreading of carbon dioxide in subsurface aquifers, Nat. Commun. **5**, 5743 (2014).

[15] V. Loodts, L. Rongy, and A. De Wit, Chemical control of dissolution-driven convection in partially miscible systems: Theoretical classification, Phys. Chem. Chem. Phys. **17**, 29814 (2015).

[16] V. Loodts, P. M. J. Trevelyan, L. Rongy, and A. De Wit, Density profiles around $A + B \rightarrow C$ reaction-diffusion fronts in partially miscible systems: A general classification, Phys. Rev. E **94**, 043115 (2016).

[17] C. Thomas, V. Loodts, L. Rongy, and A. De Wit, Convective dissolution of CO_2 in reactive alkaline solutions: Active role of spectator ions, Int. J. Greenhouse Gas Control **53**, 230 (2016).

[18] I. Cherezov and S. S. S. Cardoso, Acceleration of convective dissolution by chemical reaction in a Hele-Shaw cell, Phys. Chem. Chem. Phys. **18**, 23727 (2016).

[19] V. Loodts, Influence of chemical reactions on convective dissolution: a theoretical study, Ph.D. thesis, Université libre de Bruxelles, Brussels, Belgium, 2016.

[20] V. Loodts, B. Knaepen, L. Rongy, and A. De Wit, Enhanced steady-state dissolution flux in reactive convective dissolution, Phys. Chem. Chem. Phys. **19**, 18565 (2017).

[21] P. Ghoshal, M. C. Kim, and S. S. S. Cardoso, Reactive-convective dissolution in a porous medium: The storage of carbon dioxide in saline aquifers, Phys. Chem. Chem. Phys. **19**, 644 (2017).

[22] C. Wylock, A. Rednikov, P. Colinet, and B. Haut, Experimental and numerical analysis of buoyancy-induced instability during CO_2 absorption in $NaHCO_3$-Na_2CO_3 aqueous solutions, Chem. Eng. Sc. **157**, 232 (2017).
[23] M. A. Budroni, C. Thomas, and A. De Wit, Chemical control of dissolution-driven convection in partially miscible systems: Nonlinear simulations and experiments, Phys. Chem. Chem. Phys. **19**, 7936 (2017).
[24] V. Loodts, H. Saghou, B. Knaepen, L. Rongy, and A. De Wit, Differential diffusivity effects in reactive convective dissolution, Fluids **3**, 83 (2018).
[25] M. C. Kim and S. S. S. Cardoso, Diffusivity ratio effect on the onset of the buoyancy-driven instability of an $A + B \rightarrow C$ chemical reaction system in a Hele-Shaw cell: Asymptotic and linear stability analyses, Phys. Fluids **30**, 094102 (2018).
[26] M. Jotkar, A. De Wit, and L. Rongy, Enhanced convective dissolution due to an $A + B \rightarrow C$ reaction: Control of the nonlinear dynamics via solutal density contributions, Phys. Chem. Chem. Phys. **21**, 6432 (2019).
[27] T. Lei and K. H. Luo, Pore-scale study of dissolution-driven density instability with reaction $A + B \rightarrow C$ in porous media, Phys. Rev. Fluids **4**, 063907 (2019).
[28] A. De Wit, Chemo-hydrodynamic patterns and instabilities, Annu. Rev. Fluid Mech. **52**, 531 (2020).
[29] R. W. Griffiths, Layered double-diffusive convection in porous media, J. Fluid Mech. **102**, 221 (1981).
[30] H. E. Huppert and J. S. Turner, Double-diffusive convection, J. Fluid Mech. **106**, 299 (1981).
[31] P. M. J. Trevelyan, C. Almarcha, and A. De Wit, Buoyancy-driven instabilities of miscible two-layer stratifications in porous media and Hele-Shaw cells, J. Fluid Mech. **670**, 38 (2011).
[32] J. Carballido-Landeira, P. M. J. Trevelyan, C. Almarcha, and A. De Wit, Mixed-mode instability of a miscible interface due to coupling between Rayleigh-Taylor and double-diffusive convective modes, Phys. Fluids **25**, 024107 (2013).
[33] S. M. J. Raad, H. Hassanzadeh, and J. Ennis-King, On the dynamics of two-component convective dissolution in porous media, Water Resourc. **55**, 4030 (2019).
[34] M. C. Kim and S. S. S. Cardoso, Diffusivity ratio effect on the onset of the buoyancy-driven instability of an $A + B \rightarrow C$ chemical reaction system in a Hele-Shaw cell: Numerical simulations and comparison with experiments, Phys. Fluids **31**, 084101 (2019).
[35] T. Lei and K. H. Luo, Differential diffusion effects on density-driven instability of reactive flows in porous media, Phys. Rev. Fluids **5**, 033903 (2020).
[36] M. Bestehorn and A. Firoozabadi, Effect of fluctuations on the onset of density-driven convection in porous media, Phys. Fluids **24**, 114102 (2012).
[37] N. Tilton, D. Daniel, and A. Riaz, The initial transient period of gravitionally unstable diffusive boundary layers developing in porous media, Phys. Fluids **25**, 092107 (2013).
[38] M. Jotkar, L. Rongy, and A. De Wit, Chemically-driven convective dissolution, Phys. Chem. Chem. Phys. **21**, 19054 (2019).
[39] V. Moureau, P. Domingo, L. Vervisch, and A. Riaz, Design of a massively parallel CFD code for complex geometries, C. R. Mech. **339**, 141 (2011).